ECS Journal of Solid State
Science and Technology

Threshold Ion Energies and Cleaning of Etch Residues During Inductively Coupled Etching of NiO/Ga_2O_3 in BCl_3

To cite this article: Chao-Ching Chiang *et al* 2022 *ECS J. Solid State Sci. Technol.* **11** 115005

View the article online for updates and enhancements.

This content was downloaded from IP address 128.227.171.77 on 28/01/2023 at 01:05

ECS Journal of Solid State Science and Technology, 2022 **11** 115005
2162-8777/2022/11(11)/115005/5/$40.00 © 2022 The Electrochemical Society ("ECS"). Published on behalf of ECS by IOP Publishing Limited

Threshold Ion Energies and Cleaning of Etch Residues During Inductively Coupled Etching of NiO/Ga_2O_3 in BCl_3

Chao-Ching Chiang,[1] Xinyi Xia,[1] Jian-Sian Li,[1] Fan Ren,[1,*] and S. J. Pearton[2,*,z]

[1]*Department of Chemical Engineering, University of Florida, Gainesville, Florida 32606, United States of America*
[2]*Department of Materials Science and Engineering, University of Florida, Gainesville, Florida 32606 United States of America*

BCl_3 is an attractive plasma etchant for oxides because it is a Lewis acid used to scavenge native oxides on many semiconductors due to the strong B–O bonding. We investigated BCl_3-based dry etching of the NiO/Ga_2O_3 heterojunction system. BCl_3/Ar Inductively Coupled Plasmas produced maximum etch rates for NiO up to 300 Å.min^{-1} and 800 Å.min^{-1} for β-Ga_2O_3 under moderate plasma power conditions suitable for low damage pattern transfer. The selectivity for NiO: Ga_2O_3 was <1 under all conditions. The ion energy threshold for initiation of etching of NiO was between 35–60 eV, depending on the condition and the etch mechanism was ion-driven, as determined by the linear dependence of etch rate on the square root of ion energy incident on the surface. By sharp contrast, the etching of Ga_2O_3 had a stronger chemical component, without a well-defined ion energy threshold. The as-etched NiO and Ga_2O_3 surfaces show chlorine residues, which can be removed on both materials by the standard $1NH_4OH$: $10H_2O$ or 1HCl: $10H_2O$ rinses used for native oxide removal. According to the location of the Cl $2p_{3/2}$ peak, the Cl is ionically bonded.
© 2022 The Electrochemical Society ("ECS"). Published on behalf of ECS by IOP Publishing Limited. [DOI: 10.1149/2162-8777/ac9ff3]

Manuscript submitted October 2, 2022; revised manuscript received November 1, 2022. Published November 11, 2022.

One of the major drawbacks of β-Ga_2O_3 is the lack of p-type dopants with shallow ionization energies.[1–4] This means that at room temperature, the maximum hole concentration is impractically low, although, native p-type conductivity can be observed at high temperatures due to native Ga vacancies (V_{Ga}), which are acceptors.[3,5–7] An alternative approach is to use p-type oxides such as Cu_2O[8] or NiO[9–11] to form heterojunctions with n-type Ga_2O_3. In particular, the NiO provides a relatively wide process window, where the electrical properties can be tuned by the deposition parameters.[12,13] Both power rectifiers[10,11,14–23] and UV photodetectors[9] have been demonstrated in this system. Common to any device structure is the need to pattern the NiO and possibly the Ga_2O_3. There are some initial studies of dry etching of Ga_2O_3 but little on heterojunctions with NiO or on the etch residues remaining on the surface.[24–28] Etch rates of NiO were reported to be only 100 nm.min^{-1} in Inductively Coupled Plasmas (ICP) using Cl_2/Ar or BCl_3/Ar chemistries.[29] Instead of the Cl_2 plasma chemistry typically used for Ga_2O_3,[30–32] substitution with BCl_3 gas should have advantages because the B–O bonding of 8.39 eV is much stronger than the Cl–O bonding of 2.82 eV. The latter is too weak to form a reactive layer with oxygen in metal oxides.[33] This means that BCl_3 is widely employed to remove native oxides on semiconductors and prevent incubation delays where the prevalent chlorine plasma cannot break through the native oxide.[34]

In this paper we report the threshold ion energies for dry etching of NiO in BCl_3 discharges, the selectivity to β-Ga_2O_3, and the cleaning of chlorine-based residues remaining on the surface after plasma exposure. There was a threshold ion energy of ~35–60 eV for NiO dry etching, whereas Ga_2O_3 did not have discernable ion energy for initiation of etching, suggesting a stronger chemical etching component. Finally, standard surface cleaning steps were found to be effective in removing chlorine residues from the etched surfaces of both NiO and Ga_2O_3.

Experimental

The 190 nm thick NiO layers were deposited by magnetron sputtering on glass slides in a Kurt Lesker system at 3 mTorr working pressure and 150 W of 13.56 MHz power using two targets to achieve a deposition rate around 2 Å.sec^{-1}. The O_2/Ar gas ratio was 1/10, producing polycrystalline films with bandgap 3.75 eV, resistivity 0.1 Ω.cm, and density 5.6 g.cm^{-3}. The β-Ga_2O_3 samples used were (100) bulk, Sn-doped substrates, grown by the Edge-Fed Defined Growth method and purchased from Novel Crystal Technology (Saitama, Japan). All the samples were patterned with PR1045 photoresist and etched in a PlasmaTherm 790 reactor. Discharges with 15 sccm of BCl_3 and 5 sccm of Argon at a fixed pressure of 5 mTorr were used to etch the NiO and Ga_2O_3. Etch rates were obtained by measuring the etch depth with a Tencor profilometer after the removal of the photoresist.

The near-surface composition of the NiO and Ga_2O_3 after dry etching was examined with X-ray Photoelectron Spectroscopy (XPS), using a Physical Instruments ULVAC PHI, with an Al X-ray source (energy 1486.6 eV, source power 300 W), analysis size of 100 μm diameter, a take-off angle of 50° and acceptance angle of ±7 degrees. The electron pass energy was 23.5 eV for high-resolution scans. The atomic percentages were calculated using CasaXPS software. To remove the chlorinated residues from the surface, we examined two standard cleaning mixtures, namely, $1NH_4OH$: $10H_2O$ or 1HCl: $10H_2O$ for 60 s. Both of these rinses are used for native oxide removal.

Results and Discussion

Figure 1 shows the NiO and Ga_2O_3 etch rates in the BCl_3/Ar ICP discharges as a function of ICP source power at fixed rf chuck power of 150 W. The chuck power controls the energies of the positive ions incident on the powered electrode where the samples sit, while the ICP power controls the ion density in the discharge. These ions will include Ar^+, as well as positively charged fragments of the BCl_3 molecules. As ICP power is increased the ion energy is decreased due to the increase in ion density. This is also shown in Fig. 1. The dc bias decreases from about 380 V at 200 W ICP power to ~270 V at 600 W ICP power. The ion energy is the sum of this self-bias, plus the plasma sheath potential, which is about 25 V in this system. Thus, the average ion energies decrease from about 405 eV to ~295 eV as ICP power increases from 200 to 600 W. The etch rates of both materials increase monotonically with ICP power, showing that the increased ion density more than compensates for the decrease in ion energy. The increase of the NiO and Ga_2O_3 etch rates with ICP source power is due to the increase of the positive ion density. The etch rate of NiO is smaller than that of Ga_2O_3 for all ICP powers investigated, which is consistent with a lower degree of chemical etch component.

Figures 2a and 2b show the etch rates of the two materials as a function of rf power at different ICP powers. The corresponding dc

*Electrochemical Society Fellow.
zE-mail: spear@mse.ufl.edu

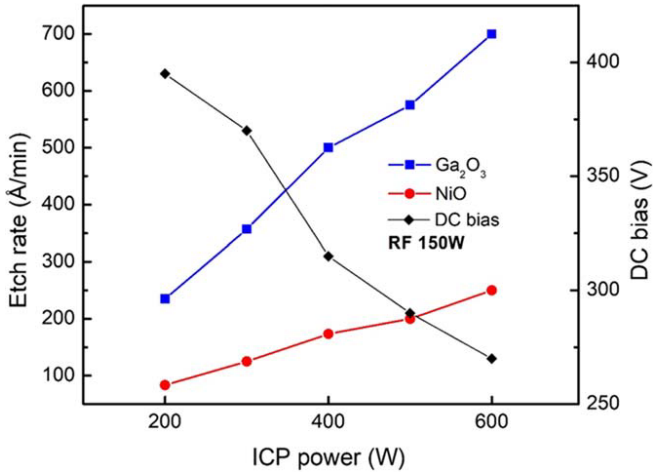

Figure 1. Etch rate of NiO and Ga_2O_3 in BCl_3/Ar discharges as a function of ICP power at fixed rf power of 150 W. The dc self-bias developed on the electrode is also shown.

self-biases are shown in Fig. 2c, showing the direct correlation of bias with rf power, with the overall magnitude reduced as ICP power is increased. The increases in etch rates with bias indicate a component of ion-driven mechanism in both cases, but the dependence is stronger for the NiO, which is consistent with the lower volatilities of the $NiCl_x$-based etch products.

The selectivity for etching one material over another is simply the ratio of their etch rates under the same conditions. Figure 3a shows the NiO/Ga_2O_3 selectivity as a function of rf power at the lowest ICP power we used, 150 W. The selectivity is essentially constant over the range of rf powers investigated. However, at higher rf powers, the selectivity increases, as shown in Fig. 3c. This shows that the ion energy is the dominant factor determining the selectivity above a certain threshold ion energy, while the selectivities are almost independent of plasma density. The selectivity for etching NiO is always <1, which is not desirable for selective patterning of NiO films on Ga_2O_3. The two approaches for overcoming this would be to use low etch rate conditions and carefully restrict the over-etch time during the plasma exposure time, or to include a thin etch stop layer between the NiO and the Ga_2O_3 which could then be selectively removed by a wet etch step.

We have reported previously that for etch processes where the ion-assisted etching mechanism is important, the etch rate (ER) is given by[35–37]

$$ER = (J_+A_{sat}(\sqrt{E} - \sqrt{E_{th}})$$

where J_+ is the positive ion flux, A_{sat} is a proportionality constant dependent on the specific plasma-material combination, E is the ion energy, and E_{th} is the threshold energy for initiation of etching. Figure 4a shows there is a linear relationship between the etch rate of both NiO and Ga_2O_3 vs the square root of ion energy. This suggests the etching for both materials is ion-flux limited.[35–37] The intercept in plots like Fig. 4a is the approximate threshold ion energy.[33] This analysis worked for the NiO, with Eth being ~35–60 eV for BCl_3/Ar in our system. These are fairly similar to the reported threshold ion energies for etching NiO in Cl_2/Ar.[28]

However, this approach did not work for Ga_2O_3 samples in Fig. 4a, where the plot has a negative intercept on the x-axis, which indicates there is also a significant chemical etching component. Similarly, under conditions of low rf power, corresponding to low ion energy, neither material showed a realistic threshold within the analysis above, since the slopes are negative in Fig. 4b. These are conditions where chemical etching plays a more significant role.

Survey XPS spectra from the two types of materials after etching and subsequent cleaning in either $1NH_4OH$: $10H_2O$ or 1HCl: $10H_2O$ rinse are shown in Fig. 5a for NiO and Fig. 5b for Ga_2O_3. It is

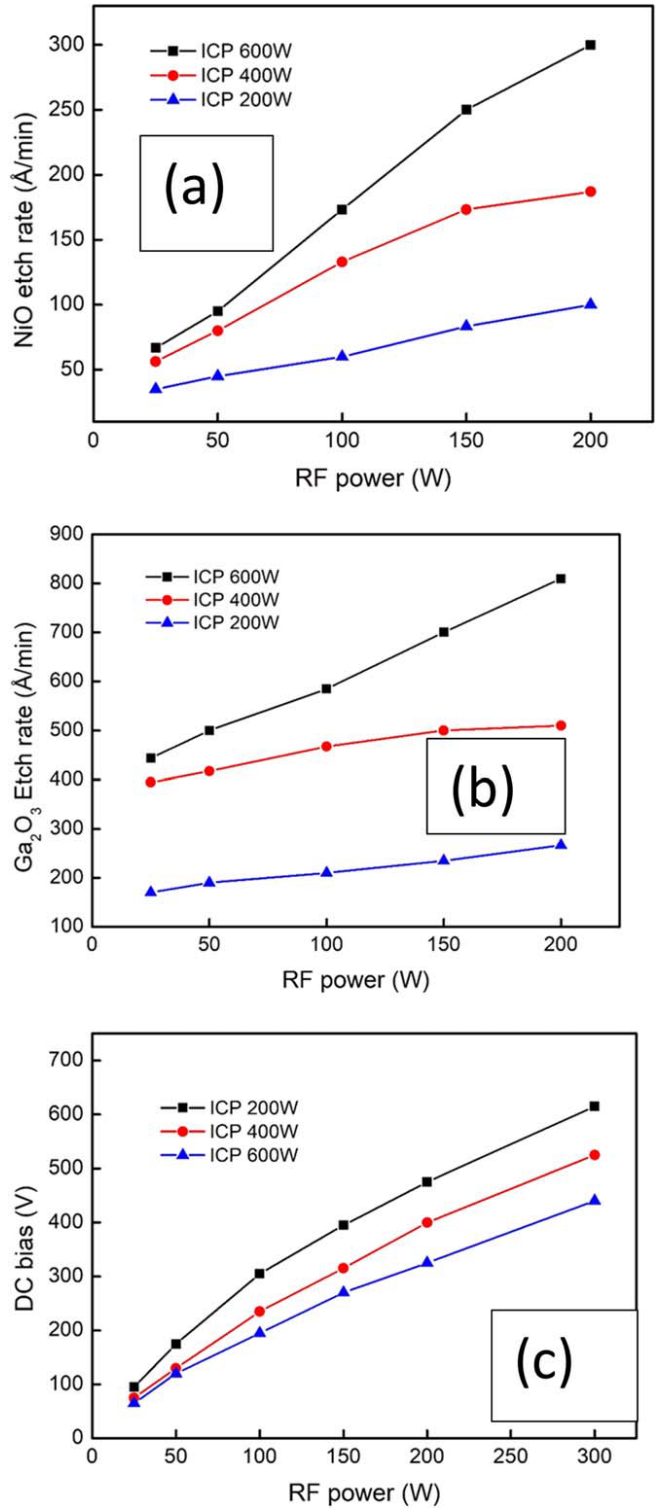

Figure 2. Etch rate of (a) NiO and (b) Ga_2O_3 in BCl_3/Ar discharges as a function of rf power at various ICP powers in the range of 200–600 W. The dc self-bias developed on the electrode is also shown in (c).

noticeable that there are small Cl-related residues on the surfaces of both materials after the BCl_3 etching. An expanded view of the Cl 2p peaks for each sample is shown in Fig. 6a for NiO and Fig. 6b for Ga_2O_3. The Cl bonds are likely to be metal bonds rather than covalent bonds according to the location of the Cl 2p peak.[38,39] Table I summarizes the near-surface atomic compositions of the samples before and after the cleaning rinses. The NiO has 15.7% Cl in this near-surface region, much higher than the 3.7% on the Ga_2O_3

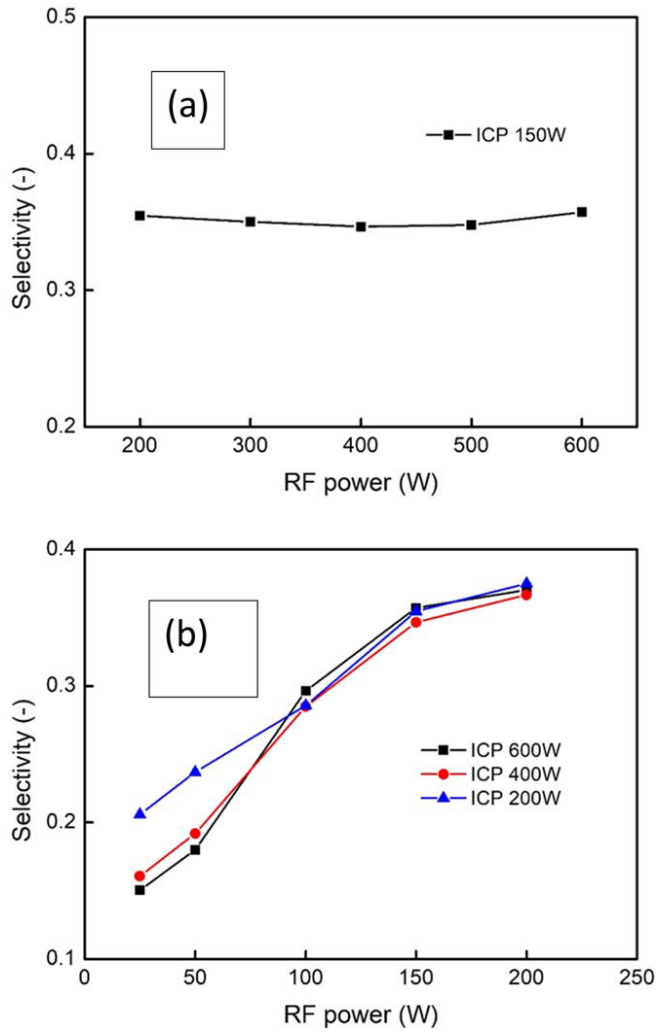

Figure 3. Etch selectivity for NiO over Ga_2O_3 in BCl_3/Ar discharges as a function of rf power for (a) ICP power of 150 W and (b) ICP powers in the range 200–600 W.

Table I. Near-surface compositions of NiO and Ga_2O_3 samples after exposure to BCl_3/Ar plasmas and then subsequent cleaning in NH_4OH or HCl rinse.

Samples	Atomic percentage (%)			
	O 1s	C 1s	Ni 2p	Cl 2p
NiO as-etched	55.42	11.07	17.81	15.70
HCl clean	62.05	8.65	29.3	0
NH_4OH clean	69.87	8.4	21.51	0.22
Samples	Atomic percentage (%)			
	O 1s	C 1s	Ga 2p3	Cl 2p
Ga_2O_3 as-etched	68.88	10.27	17.21	3.73
HCl clean	35.07	0	64.93	0
NH_4OH clean	39.27	0	60.73	0

surface. This is consistent with the lower etch rates and lower volatilities of the $NiCl_x$ etch products. Note that both cleaning procedures are effective in completely removing the chlorine-related surface residues. These are both standard processes for removing native oxides on compound semiconductor surfaces, so they fit well into any device processing sequence that includes a dry etching step.[40,41]

Summary and Conclusions

The use of NiO with n-type Ga_2O_3 has shown promising device results, but the details such as the choice of plasma chemistry for dry etching, the threshold ion energies for etching, and the subsequent surface cleaning processes have been lacking. The use of the BCl_3/Ar plasma chemistry is attractive because of the scavenging effect of this Lewis acid on native oxides. We found this chemistry

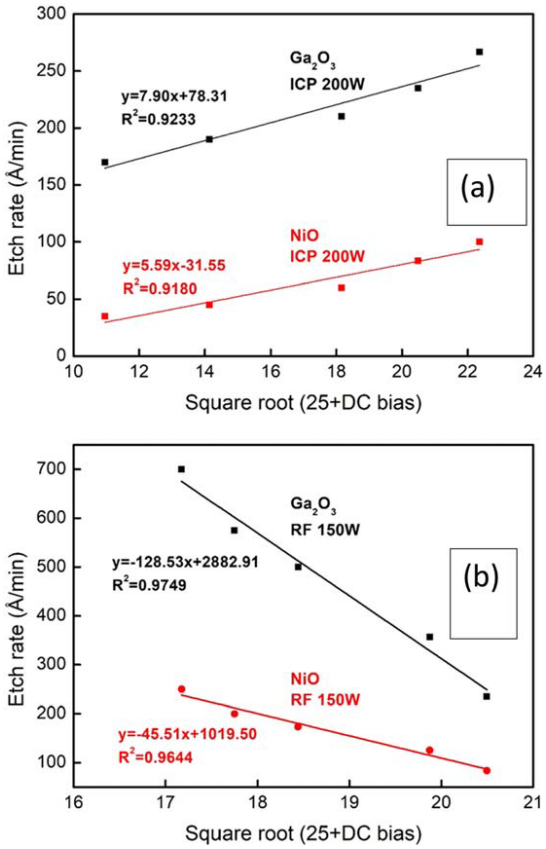

Figure 4. Etch rates for NiO and Ga_2O_3 as a function of $(25 + \text{dc bias})^{0.5}$, which approximates ion energy for (a) different RF power for fixed 200 W ICP power; (b) different ICP power for fixed 150 W RF power.

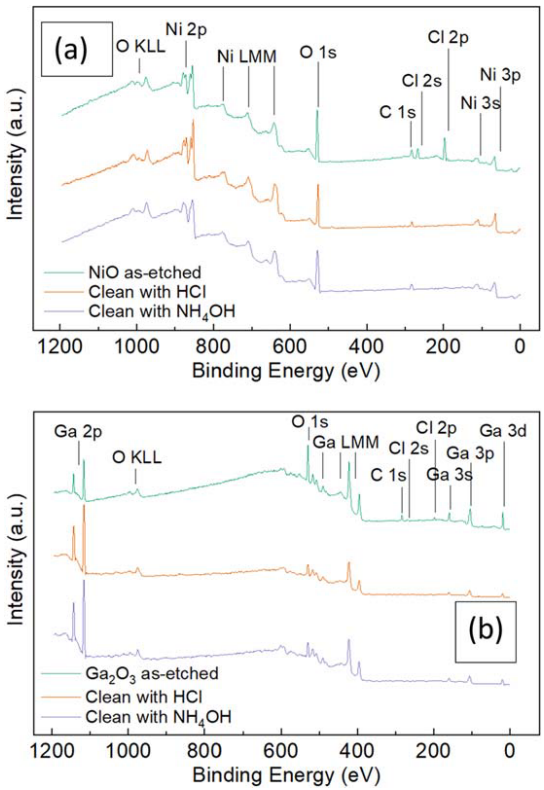

Figure 5. Survey XPS spectra from (a) NiO and (b) Ga_2O_3 after exposure to the BCl_3/Ar discharge and then subsequent cleaning in either HCl or NH_4OH.

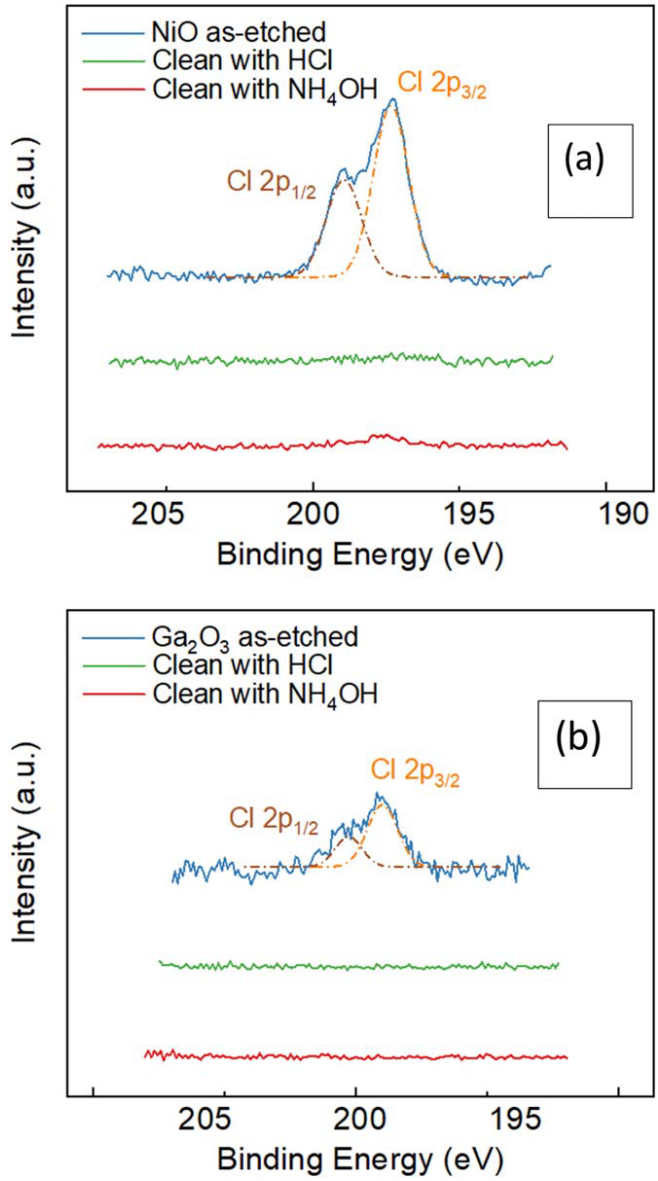

Figure 6. Expanded view of Cl 2p transitions in XPS spectra from (a) NiO and (b) Ga_2O_3 after exposure to the BCl_3/Ar discharge and then subsequent cleaning in either HCl or NH_4OH.

has selectivity <1 for NiO over Ga_2O_3, with an ion-flux-limited regime operative for NiO over a wide range of conditions. For NiO, the etch rate is independent of the reactive neural flux in the ion-flux-limited regime. Standard surface cleaning rinses were found to be effective in removing chlorinated residues. There is more scope for modification of surface properties using plasma processes, as there have been recent reports the valence and conduction band offsets of the NiO_x/β-Ga_2O_3 heterojunction decrease with F plasma pre-treatment.[40–42]

Acknowledgments

The work at UF was performed as part of Interaction of Ionizing Radiation with Matter University Research Alliance (IIRM-URA), sponsored by the Department of the Defense, Defense Threat Reduction Agency under award HDTRA1–20–2–0002. The content of the information does not necessarily reflect the position or the policy of the federal government, and no official endorsement should be inferred. The work at UF was also supported by NSF DMR 1856662 (James Edgar). The data that supports the findings of this

study are available within the article and its supplementary material. The authors have no conflicts to disclose.

ORCID

Chao-Ching Chiang https://orcid.org/0000-0002-0447-8170
Jian-Sian Li https://orcid.org/0000-0002-2817-7612
S. J. Pearton https://orcid.org/0000-0001-6498-1256

References

1. A. Mock, R. Korlacki, C. Briley, V. Darakchieva, B. Monemar, Y. Kumagai, K. Goto, M. Higashiwaki, and M. Schubert, *Phys Rev B*, **96**, 14 (2017).
2. S. I. Stepanov, V. I. Nikolaev, V. E. Bougrov, and A. E. Romanov, *Rev Adv. Mater. Sci.*, **44**, 63https://ipme.ru/e-journals/RAMS/no_14416/06_14416_stepanov.html (2016).
3. B. E. Kananen, N. C. Giles, L. E. Halliburton, G. K. Foundos, K. B. Chang, and K. T. Stevens, *J. Appl. Phys.*, **122**, 6 (2017).
4. E. Chikoidze et al., *J. Mater. Chem.*, **C7**, 10231 (2019).
5. A. Goyal, A. Zakutayev, V. Stevanović, and S. Lany, *J. Appl. Phys.*, **129**, 245704 (2021).
6. E. Chikoidze et al., *Materials Today Phys.*, **3**, 118 (2017).
7. S. Modak et al., *Appl. Phys. Lett.*, **120**, 233503 (2022).
8. S. Modak et al., *APL Mater.*, **10**, 031106 (2022).
9. T. Watahiki, Y. Yuda, A. Furukawa, M. Yamamuka, Y. Takiguchi, and S. Miyajima, *Appl. Phys. Lett.*, **111**, 222104 (2017).
10. J. Zhang, S. Han, M. Cui, X. Xu, W. Li, H. Xu, C. Jin, M. Gu, L. Chen, and K. H. L. Zhang, *ACS Appl. Electron. Mater.*, **2**, 456 (2020).
11. Y. Lv et al., *IEEE Trans. Power Electron.*, **36**, 6179 (2021).
12. H. H. Gong, X. H. Chen, Y. Xu, F.-F. Ren, S. L. Gu, and J. D. Ye, *Appl. Phys. Lett.*, **117**, 022104 (2020).
13. M. Napari, T. N. Huq, R. L. Z. Hoye, and J. L. MacManus-Driscoll, "Nickel oxide thin films grown by chemical deposition techniques: Potential and challenges in next-generation rigid and flexible device applications." *InfoMat.*, **3**, 536 (2021).
14. J. A. Spencer, A. L. Mock, A. G. Jacobs, M. Schubert, Y. Zhang, and M. J. Tadjer, *Appl. Phys. Rev.*, **9**, 011315 (2022).
15. X. Lu, X. Zhou, H. Jiang, K. W. Ng, Z. Chen, Y. Pei, K. M. Lau, and G. Wang, *IEEE Electron Dev. Lett.*, **41**, 449 (2020).
16. C. Wang et al., *IEEE Electron Dev. Lett*, **42**, 485 (2021).
17. Q. Yan et al., *Appl. Phys. Lett.*, **118**, 122102 (2021).
18. H. Gong et al., *IEEE Trans. Power Electron.*, **36**, 12213 (2021).
19. H. H. Gong et al., *Appl. Phys. Lett.*, **118**, 2021022021.
20. W. Hao, Q. He, K. Zhou, G. Xu, W. Xiong, X. Zhou, G. Jian, C. Chen, X. Zhao, and S. Long, *Appl. Phys. Lett.*, **118**, 043501 (2021).
21. F. Zhou et al., *IEEE Trans. Power Electron.*, **37**, 1223 (2022).
22. Q. Yan, H. Gong, H. Zhou, J. Zhang, J. Ye, Z. Liu, C. Wang, X. Zheng, R. Zhang, and Y. Hao, *Appl. Phys. Lett.*, **120**, 092106 (2022).
23. Y. Wang et al., *IEEE Trans. Power Electron.*, **37**, 3743 (2022).
24. J.-S. Li, C.-C. Chiang, X. Xia, F. Ren, H. Kim, and S. J. Pearton, *Appl. Phys. Lett.*, **121**, 042105 (2022).
25. J. Yang, Z. Sparks, F. Ren, S. J. Pearton, and M. Tadjer, *J. Vac. Sci. Technol. B*, **36**, 061201 (2018).
26. J. E. Hogan, S. W. Kaun, E. Ahmadi, Y. Oshima, and J. S. Speck, *Semicond. Sci. Technol.*, **31**, 065006 (2016).
27. Y. Zhang, A. Mauze, and J. S. Speck, *Appl. Phys. Lett.*, **115**, 013501 (2019).
28. C.-C. Chiang, X. Xia, J.-S. Li, F. Ren, and S. J. Pearton, *ECS J. Solid State Sci. Technol.*, **11**, 104001 (2022).
29. H. N. Cho, S. R. Min, H. J. Bae, J. H. Lee, and C. W. Chung, *Electrochem. Solid-State Lett.*, **11**, D23 (2008).
30. A. P. Shah and A. Bhattacharya, *J. Vac. Sci. Technol.*, **35**, 041301 (2017).
31. H. -C. Huang, Z. Ren, C. Chan, and X. Li, *J. Mater. Res.*, **36**, 4756 (2021).
32. H. Okumura and T. Tanaka, *Japan J. Appl. Phys.*, **58**, 120902 (2019).
33. J. B. Park, W. S. Lim, S. D. Park, B. J. Park, and G. Y. Yeom, *J. Korean Phys. Soc.*, **54**, 976 (2009).
34. *Handbook of Advanced Plasma Processing Techniques*R. J. Shul and S. J. Pearton (ed.), (Berlin)(Springer, Berlin) (2000).
35. L. Stafford, J. Margot, M. Chaker, and S. J. Pearton, *Appl. Phys. Lett.*, **87**, 071502 (2000).
36. C. Steinbruchel, *Appl. Phys. Lett.*, **55**, 1960 (1989).
37. S. J. Pearton, E. A. Douglas, R. J. Shul, and F. Ren, *J. Vac. Sci. Technol. A*, **38**, 020802 (2020).
38. C. D. Wagner, A. V. Naumkin, A. Kraut-Vass, J. W. Allison, C. J. Powell, and J. R. J. Rumble, (2003), NIST Standard Reference Database 20, Version 3.4 (web version) (http:/srdata.nist.gov/xps/).
39. I. Bello, W. H. Chang, and W. M. Lau, *J. Appl. Phys.*, **75**, 3092 (1994).
40. X. Xia, J. S. Li, C. C. Chiang, T. J. Yoo, F. Ren, H. Kim, and S. J. Pearton, *J. Phys. D*, **55**, 385105 (2022).
41. Y. Xiao, X. Li, H. Gong, W. Liu, X. Wu, S. Ding, H. Lu, and J. Ye, *Appl. Surf. Sci.*, **578**, 152047 (2022).
42. J. B. Varley, A. Janotti, C. Franchini, and C. G. Van de Walle, *Physical Review B*, **85**, 081109 (2012).